# Modulating the Shape of Short Metal-Mediated Heteroleptic Tapes of Porphyrins

Alessio Vidal,[a] Daniel Rossato,[a] Elisabetta Iengo,[a] Gabriele Balducci,[a] and Enzo Alessio*[a]

**Abstract:** In view of developing artificial light-responsive complex systems, the preparation of discrete and robust heteroleptic assemblies of different chromophores in precisely defined positions is of great value since they would allow to investigate directional processes unavailable in symmetrical architectures. Here we describe the preparation, through a modular stepwise approach, and characterization of four novel and robust metal-mediated heteroleptic $4+3$ porphyrin tapes, labeled $D_4$–$T_4$–$D_4$, $D_3$–$T_4$–$D_3$, $D_4$–$T_3$–$D_4$, and $D_3$–$T_3$–$D_3$, where a central *meso*-tetrapyridylporphyrin (either 3′-TPyP $= T_3$ or 4′-TPyP $= T_4$) is connected to two equal *cis*-dipyridylporphyrins (either 3′*cis*DPyMP $= D_3$ or 4′*cis*DPyMP $= D_4$) through four {*t,c,c*-RuCl$_2$(CO)$_2$} fragments. Whereas $D_4$–$T_4$–$D_4$ is flat, the tapes containing at least one 3′PyP, i.e. $D_3$–$T_4$–$D_3$, $D_4$–$T_3$–$D_4$, and $D_3$–$T_3$–$D_3$, have unprecedented – and well defined – 3D geometries, and each exists in solution as a pair of stereoisomers in slow conformational equilibrium. The X-ray molecular structures of two such conformers, the C-shaped $(D_3$–$T_4$–$D_3)_C$ and the z-shaped $(D_4$–$T_3$–$D_4)_z$, were determined and are fully consistent with the solution NMR findings.

## Introduction

In natural multi-chromophore systems the accomplishment of ultra-fast and precise energy and electron transfer processes requires full stereo-control on the light-absorbing units (i.e. distance and angle between adjacent chromophores). For example, in the light harvesting systems of plants and some bacteria the precise circular arrangement of chlorophyll chromophore molecules on a protein core maximizes the number of photons captured by the reaction center, thus allowing the photosynthetic process to occur.[1,2]

Therefore, in view of developing artificial light-responsive complex systems, the preparation of discrete and robust multi-porphyrin assemblies with precise control over the number and relative positioning of the chromophores, is an ambitious synthetic goal.

Organic chemistry has provided relevant contributions in this field. For example, fascinating nanorings of π-conjugated porphyrins that mimic the photosynthetic light harvesting systems were obtained by Anderson and co-workers by template-directed covalent synthesis.[3] Compared to the rela-

tively flexible linear π-conjugated porphyrin oligomers,[4–8] such symmetrical cyclic architectures afford also good topological and conformational control, which is required in artificial model structures for accurately studying their photophysical properties.[9] However, since a highly symmetrical architecture results with limitations in function, an additional synthetic challenge is the preparation of heteroleptic assemblies featuring different chromophores in precisely defined positions. Such model systems of higher structural complexity are of great value since would allow the investigation of directional processes unavailable in symmetrical architectures.[10]
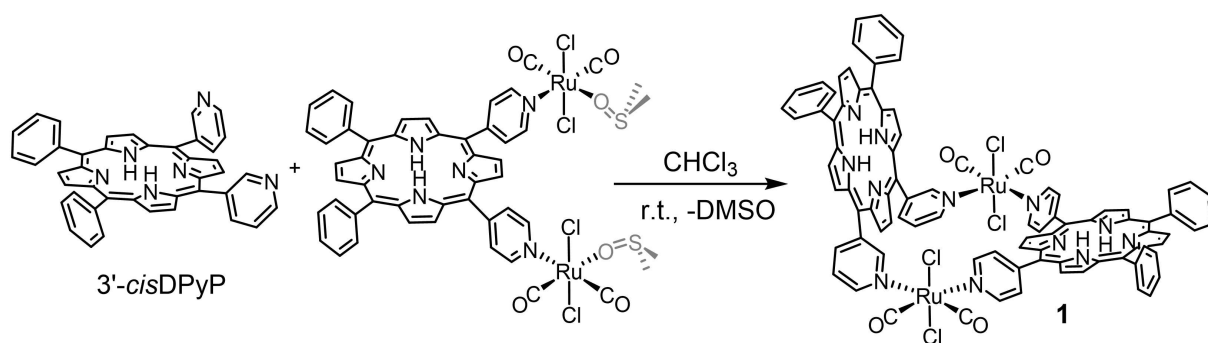
In this general context, coordination-driven self-assembly is particularly attractive as its modular nature allows one to minimize the synthetic effort while taking advantage of the strength and directionality of coordination bonds.[11–14] In the past, this synthetic strategy – often coupled with subcomponent self-assembly[15,16] – has afforded a variety of discrete and symmetrical 2D and 3D systems of the type $M_x(porp)_y$ (porp = porphyrin with peripheral donor sites), from linear assemblies to hollow cages.[17–31] However, in recent years the focus of self-assembly is also progressively shifting from homoleptic systems to more sophisticated and less symmetrical heteroleptic architectures with increased structural and functional complexity. Several strategies have been devised for achieving the non-statistical formation of the desired heteroleptic product from mixtures of individual components that are under dynamic exchange.[32–35] However, the selective assembly of more than two building blocks is particularly difficult when the reactions occur under kinetic control (e.g. with relatively inert organometallic fragments that lead to non-dynamic systems) and the individual linkers share similar features that allow no stereo-electronic discrimination. In this case, a stepwise synthetic approach is preferred for achieving full control over the stoichiometry and stereochemistry of the multi-component

[a] Dr. A. Vidal, D. Rossato, Prof. Dr. E. Iengo, Prof. Dr. G. Balducci, Prof. Dr. E. Alessio
Department of Chemical and Pharmaceutical Sciences
University of Trieste
Via L. Giorgieri 1, 34127 Trieste (Italy)
E-mail: alessio@units.it

**Chemistry–A European Journal**

Research Article
doi.org/10.1002/chem.202300893

**Chemistry Europe**
European Chemical
Societies Publishing
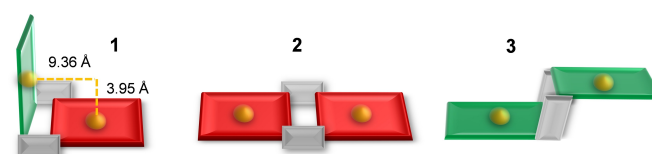
**Scheme 1.** One of the two complementary approaches for the stepwise modular preparation of the heteroleptic 2+2 metallacycle [{t,c,c-RuCl$_2$(CO)$_2$}$_2$(4'cisDPyP)(3'cisDPyP)] (**1**). The labile dmso-O ligands are in light grey.



**Figure 1.** The pictorial representation of the 2+2 neutral metallacycles of porphyrins **1** (with some relevant calculated distances), **2**, and **3**. Color code: red = 4'cisDPyP, green = 3'cisDPyP, grey = **Ru** (i.e. {t,c,c-RuCl$_2$(CO)$_2$}), gold = centroid of the porphyrin.

product, often composed of one type of metal connector and two or more different organic linkers.[36,37]

Nevertheless, to date the examples of heteroleptic metal-mediated assemblies of porphyrins are quite rare (and their characterization not always unambiguous).[22,38–44]

With the aim of contributing to this field, we recently developed a new flexible synthetic strategy that involves one type of metal connector (specifically, the 90° angular and neutral {t,c,c-RuCl$_2$(CO)$_2$} fragment, **Ru**) and two types of meso-pyridylporphyrins (PyPs) that differ in the number of meso pyridyl rings (from two to four) and/or in the position of the peripheral N atoms (4' or 3'), a feature that is very relevant in determining the geometry of the adducts.[45] As the coordination process occurs under kinetic control, our stepwise synthetic approach requires the preparation of a polytopic "acceptor" intermediate, i.e. a PyP in which each pyridyl ring is bound to the reactive ruthenium fragment {t,c,c-RuCl$_2$(CO)$_2$(dmso-O)} that has one residual easily-available coordination site temporarily occupied by the labile dmso-O. This intermediate is then treated with the second porphyrin. As a proof of concept, the novel 2+2 heteroleptic neutral metallacycle [{t,c,c-RuCl$_2$(CO)$_2$}$_2$(4'cisDPyP)(3'cisDPyP)] (**1**) was prepared by us in pure form and acceptable isolated yield through two complementary stepwise modular approaches that exploited the ditopic reactive intermediates [{t,c,c-RuCl$_2$(CO)$_2$(dmso-O)}$_2$(4'cisDPyP)] or [{t,c,c-RuCl$_2$(CO)$_2$(dmso-O)}$_2$(3'cisDPyP)] (Scheme 1).[46] Remarkably, we found that the alternative one-pot synthetic strategy, i.e. the addition of two equiv. of the ruthenium precursor [t,c,c-RuCl$_2$(CO)$_2$(dmso-O)$_2$] to a 1:1 mixture of 4'cisDPyP and 3'cisDPyP, was substantially ineffective for the preparation of **1** in pure form.
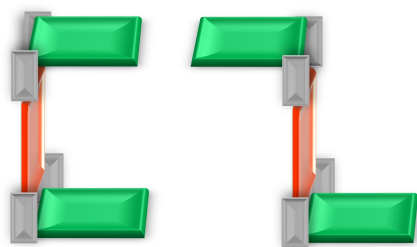
Compound **1** has an unprecedented L-shaped geometry, with the planes of the two porphyrins almost orthogonal to one another. In addition, the calculated distance from the intersection between the average planes of the two porphyrins to the centroid of 3'cisDPyP, 3.95 Å, is less than half that to the centroid of 4'cisDPyP, 9.36 Å; thus, the 4'cisDPyP side of the L-shaped metallacycle **1** is remarkably longer than the 3'cisDPyP side (Figure 1). The geometry of **1** is fully consistent with those of the corresponding homoleptic – and symmetrical – metallacycles [{t,c,c-RuCl$_2$(CO)$_2$}$_2$(4'cisDPyP)$_2$] (**2**) and [{t,c,c-

RuCl$_2$(CO)$_2$}$_2$(3'cisDPyP)$_2$] (**3**) (Figure 1), determined by us in previous years through X-ray crystallography.[47,48] A common geometrical feature in **1–3** is that the equatorial coordination plane of each **Ru** linker (N, N, C, and C) is coplanar to the porphyrin plane of 4'PyPs but almost perpendicular to that of 3'PyPs.

In this work we demonstrate that our stepwise synthetic strategy can be exploited for the preparation of four novel heteroleptic 4+3 porphyrin tapes of the type [(D)**Ru$_2$**(T)**Ru$_2$**(D)] that feature a central meso-tetrapyridylporphyrin (either 3'-TPyP = **T$_3$** or 4'-TPyP = **T$_4$**) connected to two equal cis-dipyridyl-porphyrins (either 3'cisDPyMP = **D$_3$** or 4'cisDPyMP = **D$_4$**) through four **Ru** fragments. For the sake of simplicity each neutral porphyrin tape is labeled with a string of three symbols corresponding to the three porphyrins: **D$_3$**–**T$_3$**–**D$_3$**, **D$_3$**–**T$_4$**–**D$_3$**, **D$_4$**–**T$_3$**–**D$_4$**, and **D$_4$**–**T$_4$**–**D$_4$**.[49] In addition, since porphyrins maintain a coordination geometry similar to that found in the metallacycles **1–3**, we demonstrate that the tapes containing at least one 3'PyP have unprecedented 3D geometries and each exists as two stereoisomers in slow conformational equilibrium on the NMR time scale: in one stereoisomer the two peripheral porphyrins are syn with respect to the plane of the central one, in the other they are anti. As an example, the two stereoisomers of tape **D$_3$**–**T$_4$**–**D$_3$** – one C-shaped and the other Z-shaped – are schematically shown in Figure 2.

Stepwise synthetic procedures involving polytopic "acceptor" intermediates with reactive metal centers have been exploited before in the coordination-driven construction of heteroleptic metallacycles and metallacages.[37,50–56] Nevertheless, the application of this approach to porphyrins – with their

**Chemistry–A European Journal**

Research Article
doi.org/10.1002/chem.202300893

**Chemistry Europe**
European Chemical
Societies Publishing

**Figure 2.** The pictorial representation of the two stereoisomers of tape [{t,c,c-RuCl₂(CO)₂}₄(3′cisDPyMP)₂(4′TPyP)] ($D_3$–$T_4$–$D_3$): C-shaped (left), Z-shaped (right). Color code: orange = 4′TPyP, green = 3′cisDPyP, grey = **Ru**.

peculiar chemical-physical properties and the possibility of being metallated – brings it a step further, opening the way to robust multi-chromophore assemblies with unprecedented geometries and vast potentiality.[46]

## Results and Discussion

First, by treatment of the *meso*-pyridyltolylporphyrins 3′cisD-PyMP (**D₃**) and 4′cisDPyMP (**D₄**)[45] with an excess of the Ru(II) complex [*t,c,c*-RuCl₂(CO)₂(dmso-O)₂], we prepared the two ditopic reactive intermediates [{*t,c,c*-RuCl₂(CO)₂(dmso-O)}₂(3′cisDPyMP)] (**4**) and [{*t,c,c*-RuCl₂(CO)₂(dmso-O)}₂(4′cisDPyMP)] (**5**) respectively (Figure 3) (Supporting Information, Scheme S1, Figures S1–S3). The methyl substituents on
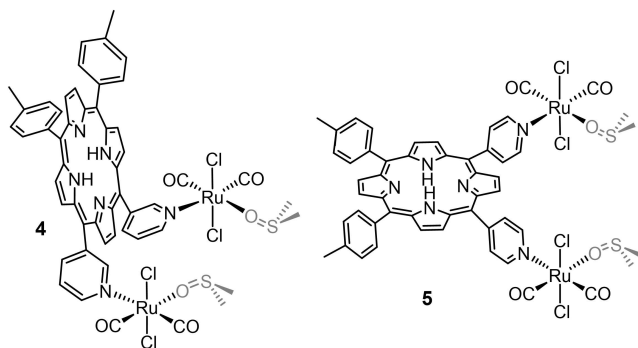


**Figure 3.** The two ditopic reactive intermediates [{*t,c,c*-RuCl₂(CO)₂(dmso-O)}₂(3′cisDPyMP)] (**4**) and [{*t,c,c*-RuCl₂(CO)₂(dmso-O)}₂(4′cisDPyMP)] (**5**). The labile dmso-O ligands are in light grey.

the phenyl rings are expected to improve the solubility of the products in chlorinated solvents and to facilitate the interpretation of the ¹H NMR spectra by reducing the number and multiplicity of the signals in the aromatic region (typically very crowded) while adding diagnostic methyl singlets in a free region.

Next, each intermediate was treated with ca. 0.5 equiv. of 4′TPyP (**T₄**) or 3′TPyP (**T₃**), for preparing the four heteroleptic tapes (Schemes S2–S5). The reactions were performed at ambient temperature in chloroform, where both **4** and **5** are well soluble, monitoring by TLC analysis the decrease of the TPyP spot. It is worth noting that each tape – despite having a much larger molecular mass – has a higher TLC mobility compared to the corresponding TPyP because all its pyridyl rings are bound to ruthenium and do not interact with the silica. The crude product was in each case purified by flash column chromatography, thus demonstrating the robustness of the tapes. Pure **D₃**–**T₄**–**D₃** and **D₄**–**T₄**–**D₄** were both obtained in very low yields (<10%), due to the scarce solubility of 4′TPyP: the initial suspension of 4′TPyP remained muddy throughout the preparation, even after the addition of **4** or **5**, thus making quite uncertain also the TLC monitoring. Attempts to improve the dissolution of 4′TPyP by heating to reflux the initial suspension for a few minutes, followed by addition of **4** or **5** after a rapid cooling, did not improve the yield significantly. The long reaction times, due to the low reactivity of 4′TPyP, had another negative consequence: in solution the [{*t,c,c*-RuCl₂(CO)₂(dmso-O)} fragments in **4** and **5** slowly undergo isomerization (that instead does not occur when **Ru** is bound to two pyridyl rings),[57] thus decreasing the selectivity of the reaction, and ultimately the yield of pure product. We found that, consistent with the literature,[58] the solubility of 4′TPyP could be improved by the addition of small amounts of trifluoroethanol (TFE), but this medium increased the isomerization rate of the ruthenium moieties in **4** and **5**, leading to complex mixtures of stereoisomers with very similar elution times and thus not amenable of chromatographic separation.

Indeed, contrary to our expectations, the geometrically simplest tape [{*t,c,c*-RuCl₂(CO)₂}₄(4′cisDPyMP)₂(4′TPyP)] (**D₄**–**T₄**–**D₄**, Figure 4), for which no stereoisomers are predicted, turned out to be the most difficult to obtain in pure form, due to its low solubility in chlorinated solvents, most likely attributable to its flat geometry leading to strong stacking interactions (Supporting Information, Figure S4).[49]
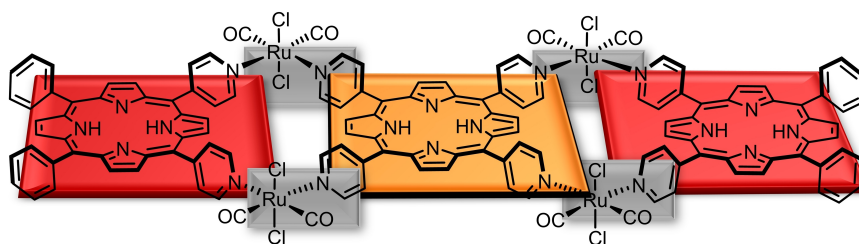


**Figure 4.** The pictorial representation of the tape [{*t,c,c*-RuCl₂(CO)₂}₄(4′cisDPyMP)₂(4′TPyP)] (**D₄**–**T₄**–**D₄**) superimposed to its schematic chemical structure. Color code: red = 4′cisDPyP, orange = 4′TPyP, grey = **Ru** (i.e. {*t,c,c*-RuCl₂(CO)₂}).

**Chemistry–A European Journal**

Research Article
doi.org/10.1002/chem.202300893

**Chemistry Europe**
European Chemical
Societies Publishing

Conversely, reactions involving 3′TPyP – that is well soluble in chloroform and thus more reactive, minimizing the above-mentioned side-reactions – afforded pure **D₄–T₃–D₄** and **D₃–T₃–D₃** in acceptable isolated yields.

The heteroleptic porphyrin tapes were fully characterized in solution by 1D and 2D NMR experiments (COSY, ROESY, HSQC, and DOSY) that, in addition to careful integration and comparison with the spectra of the 2+2 metallacycles **1** (for **D₃–T₄–D₃** and **D₄–T₃–D₄**), **2** (for **D₄–T₄–D₄**), and **3** (for **D₃–T₃–D₃**), allowed us to assign most relevant resonances unambiguously (with the exception of some overlapping signals, in particular belonging to pyrrole and tolyl protons). The coordination of the pyridyl rings to **Ru** mainly affects the resonances of the two protons adjacent to N, that typically fall in the highest frequency region of the spectrum: H2/6 (a doublet) in 4′PyPs, H2′ (a singlet) and H6′ (a doublet) in 3′PyPs. A detailed description of the assignments for each tape is reported in the Supporting Information; only some more relevant aspects of the NMR spectra are discussed below. The solution IR spectrum of each tape featured two strong CO stretching bands, consistent with the geometry of the **Ru** connectors (e.g. Figure S22). Finally, as already noted several times in our works, these neutral porphyrin adducts are not amenable for mass spectrometry investigation.[46] However, we managed to obtain the X-ray structures of the two tapes **D₃–T₄–D₃** and **D₄–T₃–D₄** that unambiguously confirmed their nature and geometry.

**Tape D₃–T₄–D₃**

We describe first the neutral **D₃–T₄–D₃** tape, [{t,c,c-RuCl₂(CO)₂}₄(3′cisDPyMP)₂(4′TPyP)], obtained by the reaction between **4** and ca. 0.5 equiv. of 4′TPyP (Supporting Information, Figures S5–S11). The ¹H NMR spectrum of the purified product shows the presence of two similar sets of signals (same number and relative intensity of the resonances) in ca. 5:1 ratio. Slow diffusion of *n*-hexane into the CDCl₃ solution afforded thin purple plate-shaped crystals that were analyzed by X-ray diffraction at the Elettra synchrotron beamline. Even though the data set was of very low quality, it nevertheless allowed us to establish unambiguously the molecular structure shown in Figure 5, corresponding to a C-shaped conformer, (**D₃–T₄–D₃**)$_C$, in which the two external *syn* 3′cisDPyMP's are ca. orthogonal to the central 4′TPyP unit (88.6° and 85.2°) and parallel to one another at a distance of 18.1 Å (measured between the centroids of the two porphyrins). The distances from the intersection between the average planes of two adjacent porphyrins to their centroids are very different: 8.9 and 9.1 Å for 4′TPyP vs 4.1 and 4.2 Å for the 3′cisDPyMP's (Figures S29 and S31). Thus, the structure of (**D₃–T₄–D₃**)$_C$ indirectly confirms also the geometry that we had predicted for the 2+2 heteroleptic metallacycle **1** (see Figure 1).[46] Each **Ru** fragment has the expected coordination sphere, with two *trans* chlorides and two adjacent carbonyls *trans* to the pyridyl rings.

We hypothesize that in solution one set of proton NMR resonances belongs to (**D₃–T₄–D₃**)$_C$, and the other to the Z-shaped *anti* conformer (**D₃–T₄–D₃**)$_Z$, in which the two peripheral
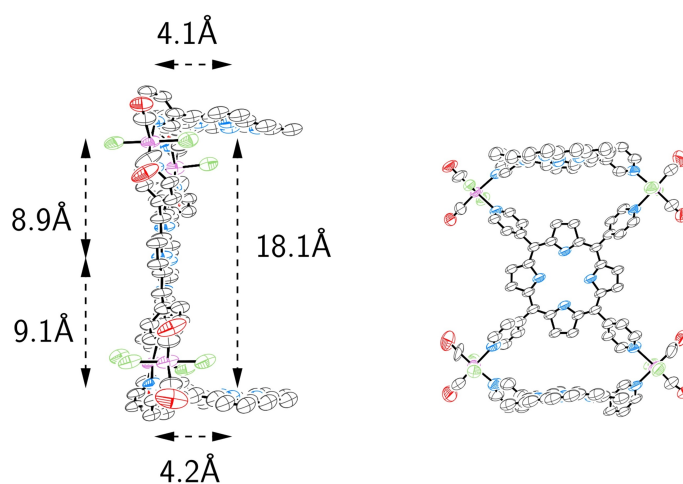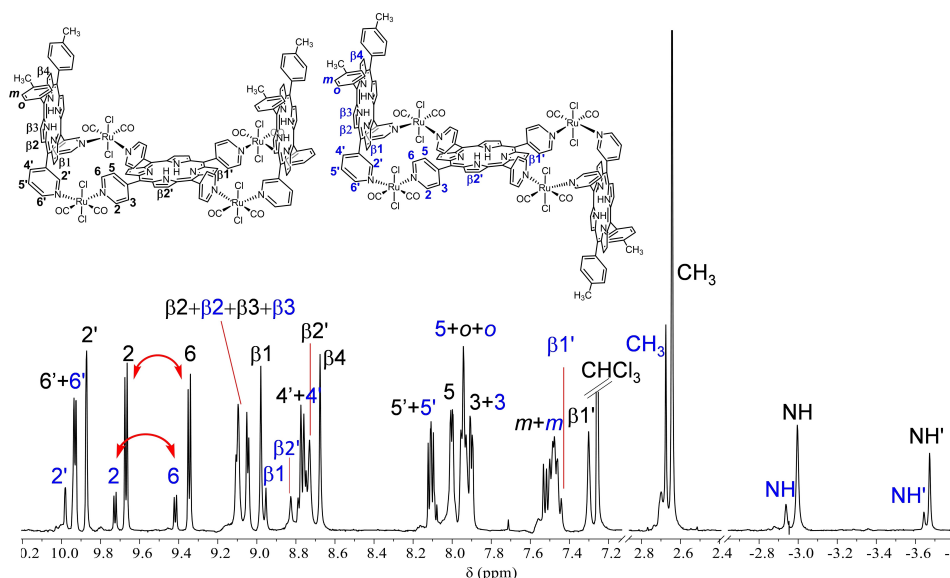


**Figure 5.** ORTEP representation (50% probability ellipsoids) of stereoisomer (**D₃–T₄–D₃**)$_C$ in the crystal structure with some significant distances. Left: side view; right: front view. Color code: N=blue, Cl=green, O=red. The *meso*-tolyl groups on the two 3′cisDPyMP's have been omitted for clarity.

porphyrins remain nearly orthogonal to the central 4′TPyP but lay on opposite sides (Figure 6).

Indeed, the two proton NMR patterns are in agreement with the proposed geometries: in both stereoisomers (**D₃–T₄–D₃**)$_C$ ($C_{2v}$ symmetry) and (**D₃–T₄–D₃**)$_Z$ ($C_{2h}$ symmetry) the two parallel 3′cisDPyMP's are symmetry-related and a vertical reflection plane makes equivalent the two halves of each porphyrin (i.e. the front and the back of the tape). Noteworthy, the high symmetry of the **Ru** fragment is instrumental for limiting the number of possible stereoisomers.

The two pairs of resolved NH singlets in the low frequency region, both with a 2:1 intensity ratio, are fully consistent with the proposed stoichiometry of the tape: the double-intensity singlets at −2.93 (minor) and −2.99 ppm (major) correspond to 4H each and belong to the two equivalent 3′cisDPyMP's, whereas the two singlets at lower frequencies (2H each) belong to the central 4′TPyP. The increased number of orthogonal macrocycles in **D₃–T₄–D₃** compared to **1** (3 vs 2) leads to an increased mutual shielding, which is particularly relevant for the central porphyrin: for example, the NH′ singlets of 4′TPyP in the two isomers of **D₃–T₄–D₃** (−3.64 and −3.67 ppm, respectively) fall at remarkably lower frequencies compared to that of 4′cisDPyP in **1** (−3.18 ppm).[46] In each set there are four equally-intense doublets for the protons on the four equivalent 4′-pyridyl rings. This typical feature is consistent with the *meso* six-membered rings laying orthogonal to the 4′TPyP plane: since this latter is not a plane of symmetry for the molecule, the proton facing the adjacent orthogonal 3′cisDPyMP (H6 in the convention adopted by us) is more shielded and thus resonates at lower frequency than the corresponding proton on the other side of the ring (H2). Slow rotation about the C$_{meso}$–C$_{ring}$ bond interconverts the pairwise equivalent protons (H6/H2 and H5/H3), and in fact their doublets are connected by exchange cross peaks in the ROESY spectrum (Figure S8). A careful examination of the COSY spectrum (Figures S5 and S6) allowed us to assign

**Chemistry–A European Journal**

Research Article
doi.org/10.1002/chem.202300893

**Chemistry Europe**
European Chemical
Societies Publishing

**Figure 6.** ^{1}H NMR spectrum (CDCl$_3$) of the mixture of the two stereoisomers of tape [{t,c,c-RuCl$_2$(CO)$_2$}$_4$(3′*cis*DPyMP)$_2$(4′TPyP)] (**D$_3$–T$_4$–D$_3$**) with the labeling scheme. The resonances of the minor isomer, attributed to (**D$_3$–T$_4$–D$_3$**)$_Z$, are labeled in blue. In both sets, primed βH and NH labels belong to the central 4′TPyP. The curved red arrows indicate resonances of exchanging protons.

the elusive resonances of the pyrrole protons βH, that often give weak correlation peaks in the HSQC spectrum: in each set the less intense NH singlet, that belongs to 4′TPyP, has two cross peaks with βH resonances, whereas the more intense NH singlet, that belongs to the 3′*cis*DPyMP's, has four such peaks. The number of cross peaks is consistent with the proposed geometries: in each isomer the pyrrole protons of 4′TPyP are expected to resonate as two singlets (β1′ and β2′), whereas those of 3′*cis*DPyMP's as two doublets (the protons between a pyridyl and a tolyl ring β2 and β3) and two singlets (β1 and β4). The assignments are consistent also with the NOE cross peaks found in the ROESY spectrum between the resonances of the pyrrole protons and those of the adjacent pyridyl and/or tolyl protons. Finally, the calculated distance between the pyrrole protons β1′ on 4′TPyP and β1 on the adjacent 3′*cis*DPyMP's (average ca. 3.8 Å) is consistent with the NOE cross peak observed in the ROESY spectrum between their resonances (Figures S8 and S9).

We were unable to establish which set of NMR resonances belongs to the crystallized stereoisomer (**D$_3$–T$_4$–D$_3$**)$_C$.[59] Nevertheless, based on chemical shift considerations, we believe that the major set of resonances can be attributed to the C-shaped isomer (**D$_3$–T$_4$–D$_3$**)$_C$ in which the two vis-a-vis 3′*cis*DPyMP's have a (small) mutual shielding contribution; consistent with this hypothesis, resonances of the major set belonging to protons facing the inside of the molecule, such as H6, H2′ and β1, resonate at slightly lower frequencies compared to the corresponding protons in the minor set.
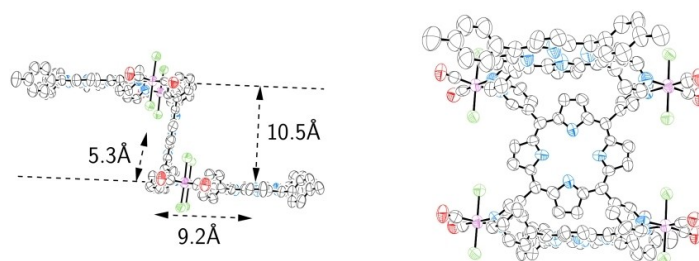
Lastly, we were interested to establish if in solution there is a conformational equilibrium between the two stereoisomers, caused by slow rotation (on the NMR time scale) of the 3′pyridyl rings about the C$_{meso}$–C$_{ring}$ bonds, as demonstrated by us for the homoleptic 2+2 metallacycle [{t,c,c-RuCl$_2$(CO)$_2$}$_2$(3′*cis*DPyP)$_2$]

(**3**).[60] Even though no intermolecular exchange cross peak was found in the room temperature ROESY spectrum, a correlation peak between the H6 doublets of (**D$_3$–T$_4$–D$_3$**)$_C$ and (**D$_3$–T$_4$–D$_3$**)$_Z$ was observed in the spectrum recorded at 50 °C (Figure S10), suggesting the presence of a very slow dynamic equilibrium between the two stereoisomers.

**Tape D$_4$–T$_3$–D$_4$**

The heteroleptic **D$_4$–T$_3$–D$_4$** tape [{t,c,c-RuCl$_2$(CO)$_2$}$_4$(4′*cis*DPyMP)$_2$(3′TPyP)] was obtained in pure form in decent isolated yield through a synthetic approach complementary to that described above, i.e. by treatment of the reactive intermediate **5** with ca. 0.5 equiv. of 3′TPyP followed by chromatographic purification (Supporting Information, Figures S12–S17). Depending on the *syn* or *anti* orientation of the two pairs of adjacent 3′-pyridyl rings on the central 3′TPyP, two limiting stereoisomers are possible also for **D$_4$–T$_3$–D$_4$**. Their expected shapes are similar to those of **D$_3$–T$_4$–D$_3$**, but – by virtue of the different geometrical features of 3′ vs 4′PyPs evidenced above and in **1** – with a smaller distance between the parallel planes of the external porphyrins. For this reason the two stereoisomers are labeled with lowercase letters, (**D$_4$–T$_3$–D$_4$**)$_c$ and (**D$_4$–T$_3$–D$_4$**)$_z$. Slow diffusion of *n*-hexane into a solution of **D$_3$–T$_4$–D$_3$** in CD$_2$Cl$_2$ afforded single crystals that, according to X-ray diffraction, in this case belonged to the z-shaped stereoisomer (Figure 7).

Notwithstanding the low quality of the diffraction data set, the structure unambiguously confirmed the nature of the compound and its main geometrical features. In (**D$_4$–T$_3$–D$_4$**)$_z$ the two symmetry-equivalent 4′*cis*DPyMP's are almost perpendicular to the 3′TPyP plane (dihedral angle 77.6°), with a slipped-

**Chemistry–A European Journal**

Research Article
doi.org/10.1002/chem.202300893

**Chemistry
Europe**
European Chemical
Societies Publishing

**Figure 7.** ORTEP representation (50% probability ellipsoids) of stereoisomer $(D_4–T_3–D_4)_z$ in the crystal structure with some significant distances. Left: side view; right: front view. Color code: N = blue, Cl = green, O = red.

cofacial geometry; the average planes through them are parallel and the interplanar distance of 10.5 Å – as anticipated – is much shorter (by ca. 40%) than in $D_3–T_4–D_3$. On the other hand, and not surprisingly, the distances from the intersection between the average planes of two adjacent porphyrins to their centroids are close to those found for $D_3–T_4–D_3$: 9.2 Å and 5.3 Å for the 4'cisDPyMP's and the central 3'TPyP, respectively (Figures S30 and S32).

The $^1$H NMR spectrum of the purified product shows two sets of resonances (ca. 1:4 ratio, Figure 8) that are similar to those of tape $D_3–T_4–D_3$ but with some significant differences, the most relevant of which concerns the singlets of the inner NH protons. In the major stereoisomer the most intense singlet (4H), that belongs to the two external 4'cisDPyMP's, falls at remarkably lower frequency compared to that of 3'TPyP (−3.72 vs −3.12 ppm), that partially overlaps with both singlets of the minor isomer. This feature suggests that the major isomer is $(D_4–T_3–D_4)_c$, where the mutual shielding of the two vis-a-vis 4'-porphyrins – due to the smaller separation – is remarkably stronger than in the $(D_3–T_4–D_3)_C$ isomer, to such an extent that the NH chemical shift order is reversed. In fact, contrary to what

found in $(D_3–T_4–D_3)_C$, in $(D_4–T_3–D_4)_c$ the NH singlet of the peripheral porphyrins falls at lower frequency than that of central one.[59] Consistently, all the resolved resonances of the protons of the two equivalent 4'cisDPyMP's of the major isomer also fall at lower frequencies than those in the minor z-shaped isomer.
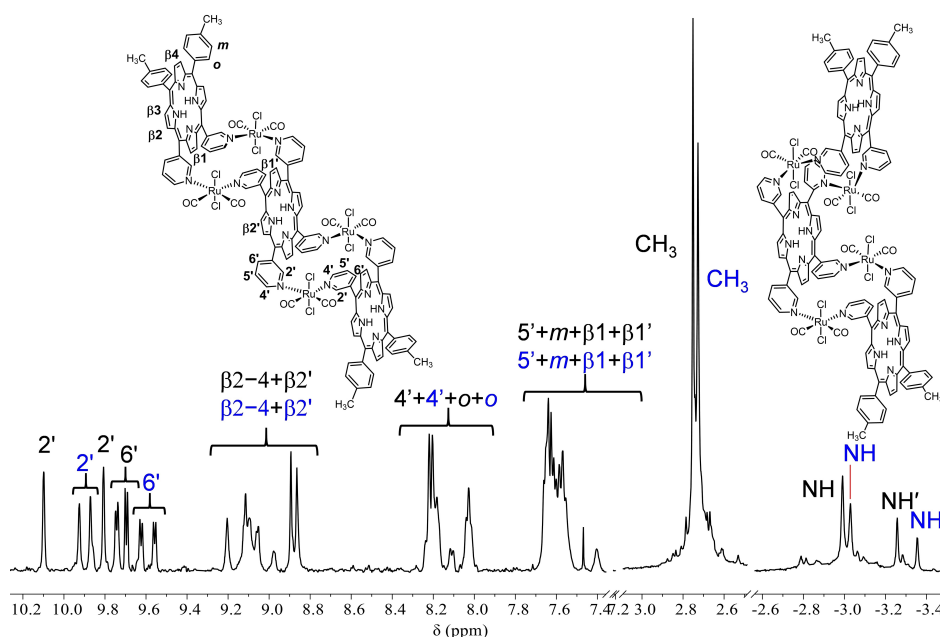
In this case no intermolecular exchange cross peak between resonances of the two sets was observed in the ROESY spectrum. However, when the sample was dissolved in $CD_2Cl_2$ the relative abundance of $(D_4–T_3–D_4)_c$ and $(D_4–T_3–D_4)_z$ was different than in CDCl$_3$ (ca. 1:2, Figures S15 and S16), suggesting that also in this case the two isomers are in slow conformational equilibrium (see also below).

**Tape $D_3–T_3–D_3$**

The $D_3–T_3–D_3$ tape, [{$t,c,c$-RuCl$_2$(CO)$_2$}$_4$(3'cisDPyMP)$_2$(3'TPyP)], was obtained in pure form and acceptable isolated yield by the reaction between **4** and 3'TPyP (Supporting Information, Figures S19–S22).
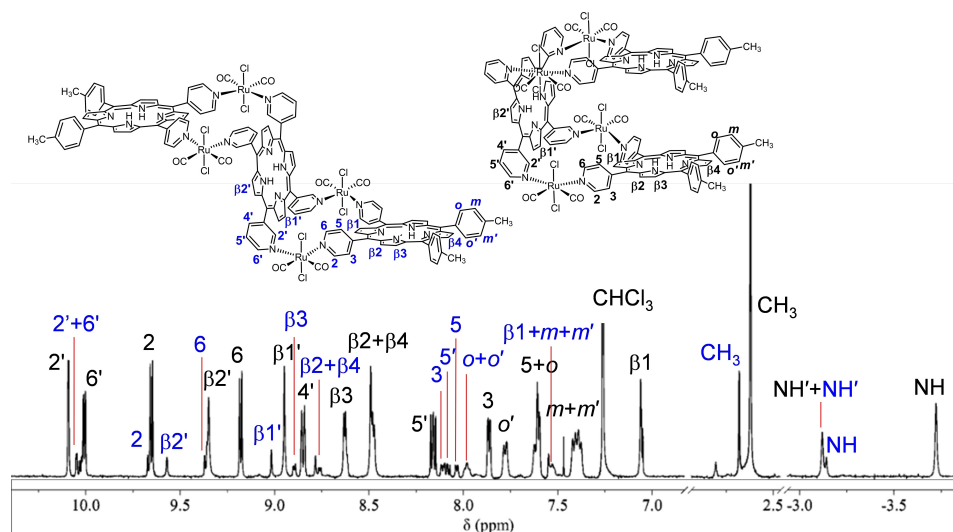


**Figure 8.** $^1$H NMR spectrum (CDCl$_3$) of the two stereoisomers of tape [{$t,c,c$-RuCl$_2$(CO)$_2$}$_4$(4'cisDPyMP)$_2$(3'TPyP)] $(D_4–T_3–D_4)$ with the labeling scheme. The resonances of the minor isomer, attributed to isomer $(D_4–T_3–D_4)_z$, are labeled in blue. In both sets, primed βH and NH labels belong to the central 3'TPyP. The CH$_3$ singlet of $(D_4–T_3–D_4)_c$ is cut.

**Chemistry–A European Journal**

Research Article
doi.org/10.1002/chem.202300893

**Chemistry Europe**
European Chemical
Societies Publishing

**Figure 9.** $^1$H NMR spectrum (CDCl$_3$) of the two stereoisomers of tape [{$t,c,c$-RuCl$_2$(CO)$_2$}$_4$(3'$cis$DPyMP)$_2$(3'TPyP)] (**D$_3$–T$_3$–D$_3$**) with the labeling scheme. The resonances of the minor isomer, whose geometry remains unassigned (see text), are labeled in blue. In both sets, primed βH and NH labels belong to protons of the central 3'TPyP. The resonances of the pyridyl protons have the same labels, regardless if they belong to 3'TPyP or to the two equivalent 3'$cis$DPyMP's (see Supporting Information for the singlets of the H2' protons).

The $^1$H NMR spectrum (Figure 9) of the purified product (single TLC spot) also contains two sets of signals (with some overlapping), indicating the presence of two different stereoisomers in solution in ca. 3:2 ratio. Consistent with the geometries of the previously discussed tapes, one stereoisomer is expected to have a *ladder* geometry, (**D$_3$–T$_3$–D$_3$**)$_L$, and the other a *Greek-frame* geometry, (**D$_3$–T$_3$–D$_3$**)$_{GF}$. In (**D$_3$–T$_3$–D$_3$**)$_{GF}$, $C_{2v}$ symmetry, all four pyridyl rings of 3'TPyP have a *syn* orientation and thus the two 3'$cis$DPyMP's are on the same side of the 3'TPyP plane, whereas in (**D$_3$–T$_3$–D$_3$**)$_L$, $C_{2h}$ symmetry, the pyridyl rings of the central 3'TPyP have a pairwise *anti* orientation and thus the peripheral porphyrins are on opposite sides of the 3'TPyP plane. The two stereoisomers have, as expected, the same number of proton resonances with similar patterns that also closely resemble that of the 2+2 homoleptic metallacycle [{$t,c,c$-RuCl$_2$(CO)$_2$}$_2$(3'$cis$DPyP)$_2$] (**3**).[48,60] The integrations of the two pairs of NH singlets confirm that each species contains the two different 3'PyPs in 2:1 ratio. Noteworthy, these are the only resonances that, based on their intensity, can be easily and unambiguously assigned to either 3'TPyP (2H) or to the two equivalent 3'$cis$DPyMP's (4H), all the other pyridyl and pyrrole resonances having (in each set) the same intensity and multiplicity. Only for the resonances of the H2' pyridyl protons (both isomers) it was also possible to distinguish between 3'TPyP and to the two equivalent 3'$cis$DPyMP's (Supporting Information).

In this case considerations on the mutual shielding among the three macrocycles did not allow us to distinguish which set of NMR signals belongs to which stereoisomer. However, the existence of a slow conformational equilibrium between them is supported by a clear exchange cross peak in the ROESY

spectrum between the two H2' resonances at 10.10 and 9.87 ppm, one belonging to (**D$_3$–T$_3$–D$_3$**)$_{GF}$ and the other (**D$_3$–T$_3$–D$_3$**)$_L$. In addition, the ratio between the two sets changed when the sample was dissolved in CD$_2$Cl$_2$, becoming nearly 1:1.

DOSY spectra were recorded for the three tapes described above (Figures S26–S28), affording the diffusion coefficients and hydrodynamic radii reported in Table 1.
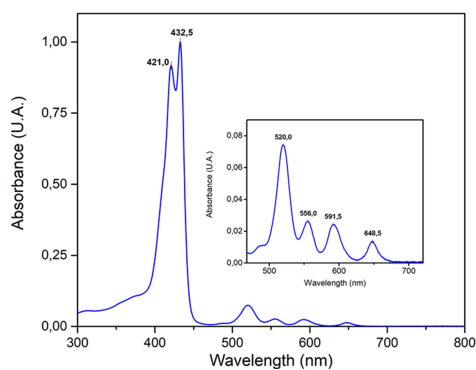
The two stereoisomers of each tape had undistinguishable diffusion coefficients. The hydrodynamic radii of the 3+4 porphyrin tapes are very similar to one another and, consistent with their size, ca. 1/3 larger than those of the smaller 2+2 metallacycles previously determined by us[46,61] and included for comparative purposes in Table 1.

As in the case of the 2+2 metallacycle **1**, the UV-vis spectra of **D$_3$–T$_4$–D$_3$** and **D$_4$–T$_3$–D$_4$** are very similar to those of the component porphyrins (Figures S11 and S17). On the contrary the spectrum of **D$_3$–T$_3$–D$_3$** showed an exciton splitting in the Soret band (Figure 10) larger than that found by us for [{$t,c,c$-RuCl$_2$(CO)$_2$}$_2$(3'$cis$DPyP)$_2$] (**3**).[48,62] This finding –

**Table 1.** Diffusion coefficients and hydrodynamic radii for the tapes determined by DOSY spectra.

| | Diffusion coefficient ×10$^6$ [cm$^2$ s$^{-1}$] | Hydrodynamic radius [Å] |
|---|---|---|
| **D$_3$–T$_4$–D$_3$** | 3.75 ± 0.06 | 10.9 |
| **D$_4$–T$_3$–D$_4$** | 3.84 ± 0.03 | 10.6 |
| **D$_3$–T$_3$–D$_3$** | 3.74 ± 0.02 | 10.9 |
| **1Zn** | 6.06 ± 0.10 | 6.7 |
| **2Zn** | 5.55 ± 0.01 | 7.3 |

*Chem. Eur. J.* **2023**, *29*, e202300893 (7 of 12)

© 2023 The Authors. Chemistry - A European Journal published by Wiley-VCH GmbH

**Figure 10.** The normalized UV-vis spectrum of tape **D₃–T₃–D₃** (CHCl₃), with an enlargement of the Q-bands in the inset.

typical for systems that feature slipped-cofacial porphyrins[63–66] – is fully consistent with the structures hypothesized for the two conformers of **D₃–T₃–D₃**, in which the three parallel porphyrins basically repeat twice the slipped-cofacial geometrical pattern of **3**.

### Host-guest chemistry

Treatment of the more abundant tapes **D₄–T₃–D₄** and **D₃–T₃–D₃** with excess zinc acetate afforded in excellent yield the corresponding fully-zincated tapes [{*t,c,c*-RuCl₂(CO)₂}₄(Zn·4'*cis*DPyMP)₂(Zn·3'TPyP)] (**ZnD₄–ZnT₃–ZnD₄**) and [{*t,c,c*-RuCl₂(CO)₂}₄(Zn·3'*cis*DPyMP)₂(Zn·3'TPyP)] (**ZnD₃–ZnT₃–ZnD₃**) (Supporting Information). Their ¹H NMR spectra are very similar to those of the parent compounds (except for the absence of the NH resonances), including the ratio between the two stereoisomers (Figures S18 and S23–S25).

Based on the X-ray structure of (**D₄–T₃–D₄**)z, and on the demonstrated capability of the embedded zinc atom to form an additional axial bond,[47] simple molecular models suggested

that 4,4'-bpy would have an almost perfect fit as a guest inside (**ZnD₄–ZnT₃–ZnD₄**)c, making two axial coordination bonds to the peripheral zinc atoms. On the other hand, the models showed that the formation of a sandwich compound, with two parallel (**ZnD₄–ZnT₃–ZnD₄**)z stereoisomers connected by three axially-bound units of 4,4'-bpy, would be disfavored by steric clashes between the two tapes. Addition of 1 equiv. of 4,4'-bpy to a CDCl₃ solution of (**ZnD₄–ZnT₃–ZnD₄**) induced remarkable changes in the ¹H NMR spectrum, fully consistent with the 100% formation of the anticipated 1:1 host-guest adduct 4,4'-bpy@(**ZnD₄–ZnT₃–ZnD₄**)c (Figure 11): 1) the resonances of the minor isomer (**ZnD₄–ZnT₃–ZnD₄**)z disappeared whereas those of the major conformer were only slightly affected in terms of chemical shift and became sharper, consistent with the host-guest equilibrium being slow on the NMR time scale; 2) in agreement with a symmetrical coordination, 4,4'-bpy gives only two upfield-shifted doublets (4H each), one at 3.95 ppm (for the inner H3,5 protons) and the other at ca. 1.4 ppm (partially overlapped by the peak of water, but clearly visible in the COSY spectrum) for the more shielded H2,6 protons; 3) integration confirms the 1:1 host-guest ratio. Thus, the formation of 4,4'-bpy@(**ZnD₄–ZnT₃–ZnD₄**)c induces the interconversion of the minor z-shaped stereoisomer into the c-shaped one, indirectly confirming the equilibrium between the two. In agreement with the geometry anticipated for 4,4'-bpy@-(**ZnD₄–ZnT₃–ZnD₄**)c, its DOSY NMR spectrum yielded an hydrodynamic radius of 9.5 Å, very similar to that of **D₄–T₃–D₄** (Table 1).

### Conclusions

We prepared, through a modular stepwise approach, a series of four neutral metal-mediated 3+4 porphyrin tapes of the type [(D)Ru₂(T)Ru₂(D)], where a central *meso*-tetrapyridylporphyrin (**T₃** or **T₄**) is connected to two equal *cis*-dipyridylporphyrins (**D₃** or **D₄**) through four {*t,c,c*-RuCl₂(CO)₂} (**Ru**) fragments. The robust compounds were obtained in pure form by column chromatography and fully characterized. Whereas [{*t,c,c*-
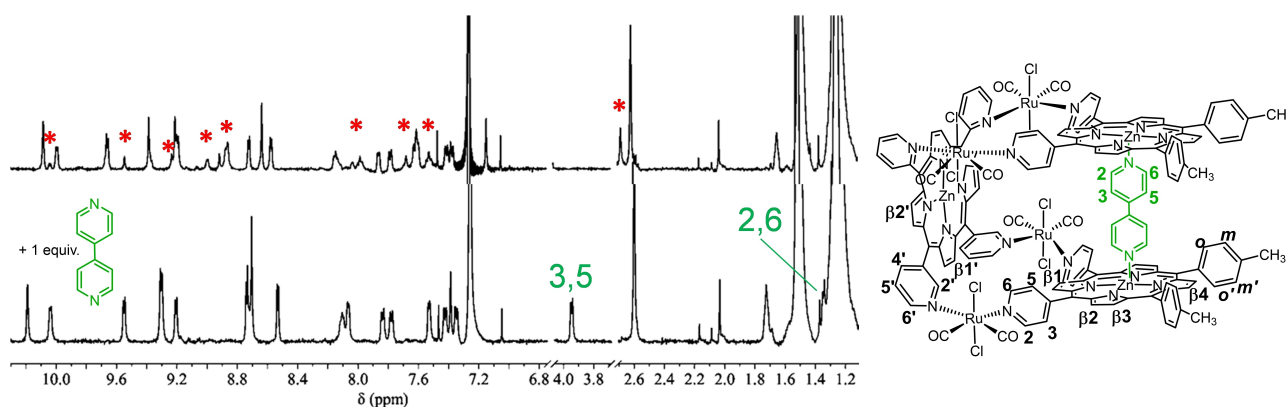


**Figure 11.** The ¹H NMR spectrum of (**ZnD₄–ZnT₃–ZnD₄**) (CDCl₃) before (top) and after the addition of 1 equiv. of 4,4'-bpy (bottom). The two resonances of 4,4'-bpy in the 1:1 host-guest adduct 4,4'-bpy@(**ZnD₄–ZnT₃–ZnD₄**)c shown on the right are labeled in green. In the top spectrum, the peaks of (**ZnD₄–ZnT₃–ZnD₄**)z, that disappear upon addition of 4,4'-bpy, are labeled with a red asterisk.

**Chemistry–A European Journal**

Research Article
doi.org/10.1002/chem.202300893

**Chemistry**
**Europe**
European Chemical
Societies Publishing

RuCl$_2$(CO)$_2$}$_4$(4'$cis$DPyMP)$_2$(4'TPyP)] (**D$_4$**–**T$_4$**–**D$_4$**) is flat (Figure 4), the tapes containing at least one 3'PyPs, that is [{$t,c,c$-RuCl$_2$(CO)$_2$}$_4$(3'$cis$DPyMP)$_2$(4'TPyP)] (**D$_3$**–**T$_4$**–**D$_3$**), [{$t,c,c$-RuCl$_2$(CO)$_2$}$_4$(4'$cis$DPyMP)$_2$(3'TPyP)] (**D$_4$**–**T$_3$**–**D$_4$**), and [{$t,c,c$-RuCl$_2$(CO)$_2$}$_4$(3'$cis$DPyMP)$_2$(3'TPyP)] (**D$_3$**–**T$_3$**–**D$_3$**), have unprecedented 3D geometries and each exists in solution as a pair of stereoisomers in slow conformational equilibrium on the NMR time scale (Figure 12). The X-ray molecular structures of two such stereoisomers, namely (**D$_3$**–**T$_4$**–**D$_3$**)$_C$ and (**D$_4$**–**T$_3$**–**D$_4$**)$_z$, were obtained and are fully consistent with the solution NMR findings.

To our knowledge, there is in the literature only one other example of similar discrete metal-mediated heteroleptic multi-porphyrin assemblies:[49] in 1998 Drain and co-workers described the one-pot formation of a square-shaped grid featuring nine $meso$ 4'-pyridylporphyrins (three different 4'PyPs in 1:4:4 ratio) connected by twelve {$t$-PdCl$_2$} fragments. Pd(II)- and Pt(II)-mediated heteroleptic tapes of porphyrins were also reported.[38] Compared to those assemblies, the heteroleptic tapes described in this work have remarkable differences: 1) They were obtained through a modular synthetic approach with a predictable outcome. 2) They were isolated in pure form, whereas the Pd(II)-mediated nonameric grid was obtained only in solution (and not isolated), and the Pd(II)- and Pt(II)-mediated tapes were obtained as mixtures of compounds with different nuclearities and characterized only through mass spectrometry. 3) Their nature and geometry are unambiguous. 4) They are truly heteroleptic, since they can incorporate porphyrins that differ not only in the number of $meso$ pyridyl rings, but also in the position of the N atom (4' vs 3'). As a consequence, we have controlled access to predictable precise geometries.

We also demonstrated that, upon metalation, the tapes can be exploited as hosts for polytopic ligands of appropriate geometry. As a proof of concept we prepared the 1:1 host-guest adduct 4,4'-bpy@(**ZnD$_4$**–**ZnT$_3$**–**ZnD$_4$**)$_C$. We anticipate that – similarly to what we did with **2Zn** and **3Zn**[47,60,61,67] – the metallated tapes might be exploited also as three-point molecular panels for the hierarchical construction of 3D multi-porphyrin assemblies with novel – and precisely predictable – geometries and increased stability owing to the larger number
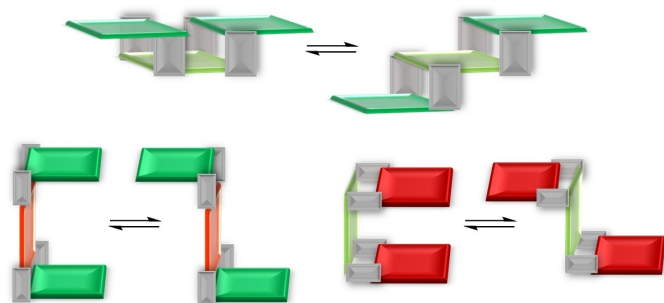
of connecting points (6 vs 4 of **2Zn** and **3Zn**). For example, treatment of 2 equiv. of **D$_3$**–**T$_3$**–**D$_3$** with 3 equiv. of a ditopic linear linker of suitable length is predicted to afford a double-decker ladder and/or Greek frame.

Finally, our modular stepwise synthetic strategy – that ultimately rests on the well-behaved Ru(II) precursor [$t,c,c$-RuCl$_2$(CO)$_2$(dmso-O)$_2$] that allows for the stepwise replacement of the two labile dmso-O ligands[68] – opens the way to exciting perspectives. For example: 1) new metal-mediated multi-porphyrin heteroleptic assemblies might be designed by changing the nature and geometry of the metal fragments and/or of the porphyrins (e.g. 3' or 4' $trans$-dipyridylporphyrins and tris-pyridylporphyrins); 2) the stepwise synthetic procedure offers the capability of inserting different metal ions inside the porphyrins in precise relative positions (e.g. center vs periphery in the tapes described here), thus allowing one to investigate the directionality of photonic communication between chromophores mediated by noncovalent interactions.

## Experimental Section

**Materials**: All chemicals, including TLC silica gel plates, were purchased from Sigma-Aldrich and used as received. Solvents were of reagent grade. The Ru(II) precursor [$t,c,c$-RuCl$_2$(CO)$_2$(dmso-O)$_2$] was prepared as described by us[69] and stored in a freezer at −18 °C. The $meso$-pyridylporphyrins and the reference 2+2 metal-lacycles [{$t,c,c$-RuCl$_2$(CO)$_2$}$_2$(4'$cis$DPyP)(3'$cis$DPyP)] (**1**), [{$t,c,c$-RuCl$_2$(CO)$_2$}$_2$(4'$cis$DPyP)$_2$] (**2**), and [{$t,c,c$-RuCl$_2$(CO)$_2$}$_2$(3'$cis$DPyP)$_2$] (**3**) were prepared and purified as described in refs. [46–48].

**Caveat**: Over the years, we learned that the characterization of these neutral metallacycles of porphyrins poses several challenges. As always observed by us in the past for previous porphyrin–Ru neutral assemblies (see Refs. [46–48]), the ESI-MS spectra of the model complexes and metallacycles of porphyrins only showed peaks deriving from the fragmentation (ESI mass spectra were collected in the positive mode on a Perkin-Elmer APII spectrometer at 5600 eV). No molecular ion peak could be detected despite the many attempts. Similarly, elemental analysis – unless is performed on the crystal samples (such as those used for X-ray determinations) – is poorly significant for these systems due to the typical presence of crystallization molecules whose nature and number vary from batch to batch. In addition, crystals are typically obtained in very small amounts that do not allow us to perform other investigations (e.g. elemental analysis or NMR spectroscopy) beside the collection of X-ray diffraction data. As a consequence, unambiguous characterization of the chromatographically pure products is achieved through extensive NMR, IR, and UV-vis spectroscopic investigations and – whenever possible – through the determination of X-ray structures.

**Instrumental methods**: Mono- and bi-dimensional ($^1$H-$^1$H COSY, ROESY, and $^1$H-$^{13}$C HSQC) NMR spectra were recorded at room temperature – unless stated otherwise – on a Varian 400 or 500 spectrometer ($^1$H: 400 or 500 MHz, $^{13}$C{$^1$H}: 100.5 or 125.7 MHz). Mixing time for ROESY experiments was 100 ms, unless otherwise stated (Supporting Information). $^1$H DOSY experiments were recorded on the Varian 500 spectrometer at 25 °C (CDCl$_3$), using the Bipolar Pulse Pair Stimulated Echo with Convection Compensation Sequence implemented into the VnmrJ software. $^1$H chemical shifts were referenced to the peak of residual non-deuterated solvent (δ = 7.26 for CDCl$_3$, 5.32 for CD$_2$Cl$_2$, 2.50 for DMSO-$d_6$). Selected carbon resonances, except for carbonyls, were assigned through



**Figure 12.** Schematic representation of the two stereoisomers in slow conformational equilibrium for the 3+4 porphyrin tapes **D$_3$**–**T$_3$**–**D$_3$** (top), **D$_3$**–**T$_4$**–**D$_3$** (bottom left), and **D$_4$**–**T$_3$**–**D$_4$** (bottom right). Color code: red = 4'$cis$DPyMP, orange = 4'TPyP, green = 3'$cis$DPyMP, light green = 3'TPyP, grey = **Ru**.

## Chemistry–A European Journal

**Research Article**
doi.org/10.1002/chem.202300893

**Chemistry Europe**
European Chemical
Societies Publishing

the HSQC spectra. The UV-vis spectra were obtained on an Agilent Cary 60 spectrophotometer, using 1.0 cm path-length quartz cuvettes (3.0 mL). Infrared spectra of chloroform solutions in the CO stretching region were recorded between $CaF_2$ windows (0.5 mm spacer) on a Perkin-Elmer Fourier-transform IR/Raman 2000 instrument in the transmission mode.

**X-ray diffraction**: Data collections were performed at the X-ray diffraction beamline (XRD1) of the Elettra Synchrotron of Trieste (Italy) equipped with a Pilatus 2 M image plate detector. Collection temperature was 100 K (nitrogen stream supplied through an Oxford Cryostream 700); the wavelength of the monochromatic X-ray beam was 0.700 Å and the diffractograms were obtained with the rotating crystal method. The crystals were dipped in the cryoprotectant oil Paratone N and mounted on the goniometer head with a nylon loop. The diffraction data were indexed, integrated and scaled using the XDS suite of codes.[70] The structure was solved by the dual space algorithm implemented in the SHELXT code.[71] Fourier analysis and refinement were performed by the full-matrix least-squares methods based on $F^2$ implemented in SHELXL.[72] The Coot and SHELXLE programs were used for modeling.[73,74] Anisotropic thermal motion was allowed for all non-hydrogen atoms. Hydrogen atoms were placed at calculated positions with isotropic factors $U = 1.2 \times U_{eq}$, $U_{eq}$ being the equivalent isotropic thermal factor of the bonded non hydrogen atom. Crystal data and details of refinements are in the Supporting Information.

It seems appropriate to remark here once more that the quality of the samples of both $(D_3–T_4–D_3)_C$, and $(D_4–T_3–D_4)_Z$ compounds was extremely poor. A single crystal having acceptable diffraction properties could be found in both cases only after (literally) tenths of attempts. This had unavoidable deleterious consequences on the final results of the refinement, as evidenced (also) by the suboptimal R values. In particular, for the $(D_3–T_4–D_3)_C$ compound, extended regions of heavily disordered and poorly structured electron density had to be modeled with the Squeeze procedure as implemented in the PLATON tool.[75] The "squeezed" electronic charge was the equivalent of 447 electrons, corresponding to about 8 $CHCl_3$ solvent molecules.

## Synthesis of the complexes

**[{t,c,c-RuCl₂(CO)₂(dmso-O)}₂(3′cisDPyMP)] (4)**: The synthetic procedure is similar to that described by us for the corresponding 3′cisDPyP compound.[46] To a 240.4 mg amount of [t,c,c-RuCl₂(CO)₂(dmso-O)₂] (0.7 mmol), dissolved in 40 mL di $CHCl_3$, 100.3 mg of 3′-cisDPyMP (0.157 mmol) was added (Ru:3′-cisDPyMP ratio of 4.5). The purple solution was stirred at room temperature for 50 min, and afterward the solvent was removed under reduced pressure affording a purple solid, that was washed with $H_2O$ to remove the unreacted complex and the free DMSO and dried under vacuum. The solid was redissolved in chloroform, and dried over $Na_2SO_4$. The solution was recovered, the solvent was removed under reduced pressure, and the solid dried under vacuum. Yield 109.6 mg, 93%. $C_{52}H_{44}N_6Cl_4O_6S_2Ru_2$, $M_w = 1257.02$. ¹H NMR (DMSO-$d_6$) δ (ppm): 9.69 (d, 2H, 2′), 9.40 (d, 2H, 6′), 9.05 (dd, 2H, 4′), 8.97–8.90 (m, 8H, Hβ), 8.24 (br m, 2H, 5′), 8.13 (br d, 4H, o), 7.66 (d, 4H, m), 2.68 (s, 6H, CH₃), −2.93 (s, 2H, NH). IR (selected bands in $CHCl_3$, cm⁻¹): 2073 (νCO), 2003 (νCO).

**[{t,c,c-RuCl₂(CO)₂(dmso-O)}₂(4′cisDPyMP)] (5)**: A procedure similar to that described above for **4** was followed, using 100.8 mg of [t,c,c-RuCl₂(CO)₂(dmso-O)₂] (0.29 mmol), 41.8 mg of 4′cisDPyMP (0.065 mmol) (Ru:4′-cisDPyMP ratio of 4.5) in 20 mL of $CHCl_3$. Yield: 64.3 mg, 87%. $C_{52}H_{44}N_6Cl_4O_6S_2Ru_2$, $M_w = 1257.02$. ¹H NMR (DMSO-$d_6$) δ (ppm): 9.37 (d, 4H, 2,6), 8.92 (m, 8H, Hβ), 8.62 (d, 4H, 3,5), 8.12 (d,

4H, o), 7.66 (d, 4H, m), 2.68 (s, 6H, Me), −2.95 (s, 2H, NH). UV-vis [$CHCl_3$; $\lambda_{max}$ (nm), relative intensity (%)]: 424 (100, Soret band), 526 (5.97), 560 (2.96), 600 (2.39), 650 (1.94). IR (selected bands in $CHCl_3$, cm⁻¹): 2072 (νCO), 2002 (νCO).

**[{t,c,c-RuCl₂(CO)₂}₄(3′cisDPyMP)₂(4′TPyP)] (D₃–T₄–D₃)**: A 47.6 mg amount of 4′TPyP (0.076 mmol) was partially dissolved in 40 mL of $CHCl_3$. Prior to the addition of a 213.7 mg amount of **4** (0.17 mmol, 2.2 equiv.), the purple suspension was heated to reflux for 15 min to promote the solubilization of the 4′TPyP and then rapidly cooled to room temperature. The mixture was stirred at room temperature, monitored by TLC ($CHCl_3$:EtOH 98:2), and stopped after 17 h. The solvent was then removed under reduced pressure and the crude product purified by column chromatography (silica gel, $CHCl_3$:n-hexane 95:5). A large part of the raw material, most likely attributable to unreacted 4′TPyP and oligomeric open-chain species, remained stuck on the top of the column as a purple band. Two of the three collected fractions were found to contain the desired product and were pooled together. Yield 7.8 mg (3%). $C_{136}H_{90}N_{20}Cl_8O_8Ru_4$, $M_w = 2820.23$. ¹H NMR ($CDCl_3$), low-case m and M stand for minor and major stereoisomer, respectively; primed βH and NH labels belong to the central 4′TPyP (see also Figure 6 for the numbering scheme), δ (ppm): 9.98 (s, 4H$_m$, 2′$_m$), 9.93 (m, 4H$_m$ + 4H$_M$, 6′$_m$ + 6′$_M$), 9.87 (d, 4H$_M$, 2′$_M$), 9.73 (d, 4H$_m$, 2$_m$), 9.67 (d, 4H$_M$, 2$_M$), 9.42 (d, 4H$_m$, 6$_m$), 9.35 (d, 4H$_M$, 6$_M$), 9.10–9.02 (m, 8H$_M$ + 8H$_m$, β2$_M$ + β2$_m$ + β3$_M$ + β3$_m$), 8.98 (s, 4H$_M$, β1$_M$), 8.96 (s, 4H$_m$, β1$_m$), 8.83 (s, 4H$_m$, β2′$_m$), 8.80 (m, 4H$_m$ + 4H$_M$, 4′$_m$ + 4′$_M$), 8.73 (s, 4H$_M$, β2′$_M$), 8.68 (s, 4H$_M$, β4$_M$), 8.11 (m, 4H$_m$ + 4H$_M$, 5′$_m$ + 5′$_M$), 8.00 (d, 4H$_M$, 5$_M$), 7.98–7.86 (m, 16H$_m$ + 12H$_M$, 5$_m$ + $o_m$ + 3$_m$ + $o_M$ + 3$_M$), 7.53–7.44 (m, 8H$_m$ + 8H$_M$, $m_m$ + $m_M$), 7.44 (s, 4H$_m$, β1′$_m$), 7.30 (s, 4H$_m$, β1′$_M$), 2.68 (s, 12H$_m$, Me$_m$), 2.64 (s, 12H$_M$, Me$_M$), −2.93 (s, 4H$_m$, NH$_m$), −2.99 (s, 4H$_M$, NH$_M$), −3.64 (s, 2H$_m$, NH′$_m$), −3.67 (s, 2H$_M$, NH′$_M$). UV-vis [$CHCl_3$; $\lambda_{max}$ (nm), ($\varepsilon \times 10^4$ (cm⁻¹M⁻¹)]: 424 (71.6, Soret band), 521 (4.93), 557 (2.57), 593.5 (1.83), 649.5 (1.29). IR (selected bands in $CHCl_3$, cm⁻¹): 2067 (νCO), 2002 (νCO).

**[{t,c,c-RuCl₂(CO)₂}₄(4′cisDPyMP)₂(3′TPyP)] (D₄–T₃–D₄)**: To a 65.3 mg amount of **5** (0.052 mmol) dissolved in 20 mL of $CHCl_3$, 15.9 mg of 3′TPyP (0.026 mmol, 0.5 equiv.) was added. The purple solution was stirred at room temperature, monitored by TLC ($CHCl_3$:EtOH 98:2), and stopped after 22 h. The solvent was then removed under reduced pressure and the crude product (pre-dissolved in a $CHCl_3$: n-hexane 94:6 mixture) was purified by column chromatography (silica gel, $CHCl_3$:n-hexane 97:3). Yield 10.7 mg (15%). $C_{136}H_{90}N_{20}Cl_8O_8Ru_4$, $M_w = 2820.23$. ¹H NMR ($CDCl_3$), low-case m and M stand for minor and major stereoisomer, respectively; primed βH and NH labels belong to the central 3′TPyP (see also Figure 8 for the numbering scheme), δ (ppm): 10.09 (s, 4H$_M$, 2′$_M$), 10.05 (s, 4H$_m$, 2′$_m$), 10.03 (d, 4H$_m$, 6′$_m$), 10.01 (d, 4H$_M$, 6′$_M$), 9.66 (d, 4H$_m$, 2$_m$) 9.65 (d, 4H$_M$, 2$_M$), 9.57 (s, 4H$_m$, β2′$_m$), 9.36 (d, 4H$_m$, 6$_m$), 9.35 (s, 4H$_M$, β2′$_M$) 9.18 (d, 4H$_M$, 6$_M$), 9.02 (s, 4H$_m$, β1′$_m$), 8.95 (s, 4H$_M$, β1′$_M$), 8.89 (d, 4H$_M$, β3$_M$), 8.85 (m, 4H$_M$, 4′$_M$), 8.78 (s, 4H$_m$, β4$_m$), 8.76 (d, 4H$_m$, β2$_m$), 8.63 (d, 4H$_M$, β3$_M$), 8.52–8.43 (m, 8H$_M$, β2$_M$ + β4$_M$), 8.16 (dd, 4H$_M$, 5′$_M$), 8.11 (d, 4H$_m$, 3$_m$), 8.08 (d, 4H$_m$, 5′$_m$) 8.04 (d, 4H$_m$, 5$_m$), 7.98 (br m, 8H$_m$, $o + o'_m$), 7.86 (d, 4H$_M$, 3$_M$), 7.78 (d, 4H$_M$, $o'_M$), 7.65–7.57 (m, 8H$_M$, 5$_M$ + $o_M$), 7.54 (m, 12H$_m$, β1$_m$ + $m$ + $m'_m$) 7.40 (m, 8H$_M$, $m$ + $m'_M$), 7.06 (s, 4H$_m$, β1$_m$) 2.68 (s, 12H$_m$, Me$_m$), 2.62 (s, 12H$_M$, Me$_M$), −3.12 (s, 2H$_m$ + 2H$_M$, NH′$_m$ + NH′$_M$), −3.14 (s, 4H$_m$, NH$_m$), −3.72 (s, 4H$_M$, NH$_M$). UV-vis [$CHCl_3$; $\lambda_{max}$ (nm), ($\varepsilon \times 10^4$ (cm⁻¹M⁻¹)]: 423 (57.9, Soret band), 519 (4.2), 555 (1.96), 592 (1.95), 648 (0.83). IR (selected bands in $CHCl_3$, cm⁻¹): 2069 (νCO), 2005 (νCO). TLC R$_f$ (silica gel, $CHCl_3$): 0.10.

**[{t,c,c-RuCl₂(CO)₂}₄(Zn·4′cisDPyMP)₂(Zn·3′TPyP)] (ZnD₄–ZnT₃–ZnD₄)**: To a 10.7 mg amount of D₄–T₃–D₄ (3.79 μmol) dissolved in 10 mL of $CHCl_3$, 3.63 mg of $Zn(AcO)_2 \cdot 2H_2O$ (0.017 mmol, ca. 4.5 equiv.) dissolved in 1 mL of MeOH was added. The solution was stirred in the dark for 24 h and then washed with water (3×30 mL). The organic phase was dried on $Na_2SO_4$, the

**Chemistry–A European Journal**

Research Article
doi.org/10.1002/chem.202300893

**Chemistry Europe**
European Chemical
Societies Publishing

solvent was removed under reduced pressure and the solid dried under vacuum. Yield 10.7 mg (3.55 µmol), 94%. $C_{136}H_{84}N_{20}Cl_8O_8Ru_4Zn_3$, $M_w = 3010.32$. $^1$H NMR (CDCl$_3$), low-case m and M stand for minor and major stereoisomer, respectively; primed βH labels belong to the central 3′TPyP (see also Figure 8 for the numbering scheme), δ (ppm): 10.08 (s, 4H$_M$, 2′$_M$) 10.06 (s+d, 4H$_m$ + 4H$_m$, 2′$_m$+6′$_m$), 9,98 (d, 4H$_M$, 6′$_M$), 9.66 (2d, 4H$_M$+4H$_m$, 2$_M$+2$_m$), 9.54 (s, 4H$_m$, β2′$_m$), 9.38 (d+s, 4H$_m$+4H$_M$, 6$_m$+β2′$_M$), 9.24–9.16 (m, 8H$_M$+ 4H$_m$, 6$_M$+β1′$_M$+β1′$_m$), 9.07–8.87 (m, 12H$_m$, β2–4$_m$), 8.85 (br t, 4H$_M$, 4′$_M$), 8.72 (d, 4H$_M$, β3$_M$), 8.63 (s, 4H$_M$, β4$_M$), 8.57 (d, 4H$_M$, β2$_M$), 8.14 (br t, 4H$_M$, 5′$_M$), 8.12–7.74 (m, 20H$_m$, 5$_m$+5′$_m$+3$_m$+o$_m$+o′$_m$), 7.86 (d, 4H$_M$, 5$_M$), 7.78 (d, 4H$_M$, o′$_M$), 7.70–7.58 (m, 8H$_M$, o$_M$+3$_M$), 7.55–7.49 (m, 12H$_m$, m+m′$_m$+β1$_m$), 7.44–7.34 (d+d, 8H$_M$, m$_M$+m′$_M$), 7.14 (s, 4H$_M$, β1$_M$), 2.69 (s, 12H$_m$, Me$_m$), 2.62 (s, 12H$_M$, Me$_M$). UV-vis [CHCl$_3$; λ$_{max}$ (nm), (ε ×10$^4$ (cm$^{-1}$ M$^{-1}$)]: 427 (43.3, Soret band), 561 (2.80), 602.5 (1.08).

[{$t,c,c$-RuCl$_2$(CO)$_2$}$_4$(3′$cis$DPyMP)$_2$(3′TPyP)] (D$_3$–T$_3$–D$_3$): To a 199.0 mg amount of **4** (0.16 mmol) dissolved in 40 mL of CHCl$_3$ a 49.5 mg amount of 3′TPyP (0.08 mmol) was added. The purple solution was stirred at room temperature, monitored by silica gel TLC (CHCl$_3$:EtOH 98:2), and stopped after 18 h. The solvent was then removed under reduced pressure and the crude product (pre-dissolved in a CHCl$_3$:$n$-hexane 94:6 mixture) was purified by column chromatography (silica gel, CHCl$_3$:$n$-hexane 97:3). One main fraction was collected. Yield 50.6 mg (23%). $C_{136}H_{90}N_{20}Cl_8O_8Ru_4$, $M_w = 2820.23$. $^1$H NMR (CDCl$_3$), low-case m and M stand for minor and major stereoisomer, respectively; primed βH and NH labels belong to the central 3′TPyP (see also Figure 9 for the numbering scheme), δ (ppm): 10.10 (s, H$_M$, 2′$_M$), 9.92 (s, 4H$_m$, 2′$_m$) 9.87 (s, 4H$_m$, 2′$_m$), 9.81 (s, 4H$_M$, 2′$_M$), 9.74 (d, 4H$_M$, 6′$_M$), 9.69 (d, 4H$_M$, 6′$_M$), 9.62 (d, 4H$_m$, 6′$_m$), 9.56 (d, 4H$_m$, 6′$_m$), 9.27–8.83 (m, 16H$_M$+16H$_m$, β2–4$_M$+β2′$_M$+β2–4$_m$+β2′$_m$), 8.28–7.96 (m, 16H$_M$+16H$_m$, 4′$_M$+4′$_m$+o$_M$+o$_m$), 7.74–7.30 (m, 24H$_M$+24H$_m$, 5′$_M$+m$_M$+β1$_M$+β1′$_M$+5′$_m$+m$_m$+β1$_m$+β1′$_m$), 2.75 (s, 12H$_M$, Me$_M$), 2.73 (s, 12H$_m$, Me$_m$), −2.99 (s, 4H$_M$, NH$_M$), −3.03 (s, 4H$_m$, NH$_m$), −3.26 (s, 2H$_M$, NH′$_M$), −3.36 (s, 2H$_m$, NH′$_m$). UV-vis [CHCl$_3$; λ$_{max}$ (nm), (ε ×10$^4$ (cm$^{-1}$ M$^{-1}$)]: 420.5 (50.4, Soret band), 433 (54.8, Soret band), 520.5 (4.93), 555 (1.79), 591.5 (1.58), 647 (0.93). IR (selected bands in CHCl$_3$, cm$^{-1}$): 2074 (νCO), 2014 (νCO). TLC R$_f$ (CHCl$_3$) = 0.12.

**Supporting Information**: Additional comments on the preparation and spectroscopic characterization of the reactive intermediates and tapes, mono- and bidimensional and DOSY NMR spectra, IR and UV-visible spectra for the reported compounds. Details of X-ray data collection and refinement for compounds (D$_3$–T$_4$–D$_3$)$_C$ and (D$_4$–T$_3$–D$_4$)$_Z$. This material is available free of charge via the Internet at http://pubs.acs.org.

### Accession Codes

Deposition Number(s) 2244872 ((D$_4$–T$_3$–D$_4$)$_Z$) and 2244873 ((D$_3$–T$_4$–D$_3$)$_C$) contain(s) the supplementary crystallographic data for this paper. These data are provided free of charge by the joint Cambridge Crystallographic Data Centre and Fachinformationszentrum Karlsruhe Access Structures service.

## Conflict of Interests

The authors declare no conflict of interest.

## Data Availability Statement

The data that support the findings of this study are available from the corresponding author upon reasonable request.

[1] Y. Umena, K. Kawakami, J.-R. Shen, N. Kamiya, *Nature* **2011**, *473*, 55–59.
[2] K. Tani, R. Kanno, X.-C. Ji, M. Hall, L.-J. Yu, Y. Kimura, M. T. Madigan, A. Mizoguchi, B. M. Humbel, Z.-Y. Wang-Otomo, *Biochem.* **2021**, *60*, 2483–2491.
[3] P. S. Bols, H. L. Anderson, *Acc. Chem. Res.* **2018**, *51*, 2083–2092.
[4] M. J. Crossley, P. L. Burn, *J. Chem. Soc. Chem. Commun.* **1991**, 1569–1571.
[5] H. L. Anderson, *Inorg. Chem.* **1994**, *33*, 972–981.
[6] V. S.-Y. Lin, S. G. DiMagno, M. J. Therien, *Science* **1994**, *264*, 1105–1111.
[7] P. N. Taylor, J. Huuskonen, G. Rumbles, R. T. Aplin, E. Williams, H. L. Anderson, *Chem. Commun.* **1998**, 909–910.
[8] H. L. Anderson, *Chem. Commun.* **1999**, 2323–2331.
[9] J. K. Sprafke, D. V. Kondratuk, M. Wykes, A. L. Thompson, M. Hoffmann, R. Drevinskas, W.-H. Chen, C. K. Yong, J. Kärnbratt, J. E. Bullock, M. Malfois, M. R. Wasielewski, B. Albinsson, L. M. Herz, D. Zigmantas, D. Beljonne, H. L. Anderson, *J. Am. Chem. Soc.* **2011**, *133*, 17262–17273.
[10] A. Prodi, C. Chiorboli, F. Scandola, E. Iengo, E. Alessio, R. Dobrawa, F. Würthner, *J. Am. Chem. Soc.* **2005**, *127*, 1454–1462.
[11] B. J. Holiday, C. A. Mirkin, *Angew. Chem. Int. Ed.* **2001**, *40*, 2022–2043; *Angew. Chem.* **2001**, *113*, 2076–2097.
[12] M. M. Safont-Sempere, G. Fernández, F. Würthner, *Chem. Rev.* **2011**, *111*, 5784–5814.
[13] R. Chakrabarty, P. S. Mukherjee, P. J. Stang, *Chem. Rev.* **2011**, *111*, 6810–6918.
[14] S. Mukherjee, P. S. Mukherjee, *Chem. Commun.* **2014**, *50*, 2239–2248.
[15] T. K. Ronson, S. Zarra, S. P. Black, J. R. Nitschke, *Chem. Commun.* **2013**, *49*, 2476–2490.
[16] D. Zhang, T. K. Ronson, J. R. Nitschke, *Acc. Chem. Res.* **2018**, *51*, 2423–2436.
[17] E. G. Percástegui, V. Jancik, *Coord. Chem. Rev.* **2020**, *407*, 213165.
[18] S. Durot, J. Taesch, V. Heitz, *Chem. Rev.* **2014**, *114*, 8542–8578.
[19] E. Iengo, P. Cavigli, D. Milano, P. Tecilla, *Inorg. Chim. Acta* **2014**, *417*, 59–78.
[20] E. Iengo, E. Zangrando, E. Alessio, *Acc. Chem. Res.* **2006**, *39*, 841–851.
[21] C. M. Drain, J.-M. Lehn, *J. Chem. Soc., Chem. Commun.* **1994**, 2313–2315.
[22] R. V. Slone, J. T. Hupp, *Inorg. Chem.* **1997**, *36*, 5422–5423.
[23] P. J. Stang, J. Fan, B. Olenyuk, *Chem. Commun.* **1997**, 1453–1454.
[24] N. Fujita, K. Birhadha, M. Fujita, S. Sakamoto, K. Yamaguchi, *Angew. Chem. Int. Ed.* **2001**, *40*, 1718–1721; *Angew. Chem.* **2001**, *113*, 1768–1771.
[25] A. K. Bar, R. Chakrabarty, G. Mostafa, P. S. Mukherjee, *Angew. Chem. Int. Ed.* **2008**, *47*, 8455–8459; *Angew. Chem.* **2008**, *120*, 8583–8587.
[26] L. P. Hernández, A. González-Álvarez, A. I. Oliva, P. Ballester, *J. Porphyrins Phthalocyanines* **2009**, *13*, 481–493.
[27] W. J. Meng, B. Breiner, K. Rissanen, J. D. Thoburn, J. K. Clegg, J. R. Nitschke, *Angew. Chem. Int. Ed.* **2011**, *50*, 3479–3483; *Angew. Chem.* **2011**, *123*, 3541–3545.
[28] A. K. Bar, S. Mohapatra, E. Zangrando, P. S. Mukherjee, *Chem. Eur. J.* **2012**, *18*, 9571–9579.
[29] D. M. Wood, W. Meng, T. K. Ronson, A. R. Stefankiewicz, J. K. Sanders, J. R. Nitschke, *Angew. Chem. Int. Ed.* **2015**, *54*, 3988–3992; *Angew. Chem.* **2015**, *127*, 4060–4064.
[30] F. J. Rizzuto, J. R. Nitschke, *Nat. Chem.* **2017**, *9*, 903–908.
[31] J. A. Wytko, R. Ruppert, C. Jeandon, J. Weiss, *Chem. Commun.* **2018**, *54*, 1550–1558.
[32] M. Yoshizawa, M. Nagao, K. Kumazawa, M. Fujita, *J. Organomet. Chem.* **2005**, *690*, 5383–5388.

[33] S. De, K. Mahata, M. Schmittel, *Chem. Soc. Rev.* **2010**, *39*, 1555–1575.

[34] Z. He, W. Jiang, C. A. Schalley, *Chem. Soc. Rev.* **2015**, *44*, 779–789.

[35] S. Pullen, J. Tessarolo, G. H. Clever *Chem. Sci.* **2021**, *12*, 7269–7293.

[36] G. Vantomme, E. W. Meijer, *Science* **2019**, *363*, 1396–1397.

[37] Y. Sun, C. Chen, J. Liuc, P. J. Stang, *Chem. Soc. Rev.* **2020**, *49*, 3889–3919.

[38] C. M. Drain, F. Nifiatis, A. Vasenko, J. D. Batteas, *Angew. Chem. Int. Ed.* **1998**, *37*, 2344–2347; *Angew. Chem.* **1998**, *110*, 2478–2481.

[39] K. F. Cheng, N. A. Thai, K. Grohmann, L. C. Teague, C. M. Drain, *Inorg. Chem.* **2006**, *45*, 6928–6932.

[40] S. K. Samanta, D. Samanta, J. W. Bats, M. Schmittel, *J. Org. Chem.* **2011**, *76*, 7466–7473.

[41] M. Yedukondalu, M. Ravikanth, *J. Chem. Sci.* **2011**, *123*, 201–214.

[42] S. Gaikwad, M. L. Saha, D. Samanta, M. Schmittel, *Chem. Commun.* **2017**, *53*, 8034–8037.

[43] F. J. Rizzuto, W. J. Ramsay, J. R. Nitschke, *J. Am. Chem. Soc.* **2018**, *140*, 11502–11509.

[44] S. Saha, P. K. Biswas, M. Schmittel, *Inorg. Chem.* **2019**, *58*, 3466–3472.

[45] Abbreviations used in this manuscript: 4′*cis*DPyP = 5,10-bis(4′-pyridyl)-15,20-diphenylporphyrin, 4′*cis*DPyMP = 5,10-bis(4′-pyridyl)-15,20-di-*p*-(tolyl)porphyrin, 3′*cis*DPyP = 5,10-bis(3′-pyridyl)-15,20-diphenylporphyrin, 3′*cis*DPyMP = 5,10-bis(3′-pyridyl)-15,20-di-*p*(tolyl)porphyrin, 4′-TPyP = 5,10,15,20-tetra(4′-pyridyl)porphyrin, 3′-TPyP = 5,10,15,20-tetra(3′-pyridyl)porphyrin. For the sake of brevity, abbreviated versions of the geometrical descriptors for the metal centers are used in the formulas: $c = cis$, $t = trans$.

[46] A. Vidal, F. Battistin, G. Balducci, E. Iengo, E. Alessio, *Inorg. Chem.* **2021**, *60*, 11503–11513.

[47] E. Iengo, E. Zangrando, R. Minatel, E. Alessio, *J. Am. Chem. Soc.* **2002**, *124*, 1003–1013.

[48] E. Iengo, E. Zangrando, M. Bellini, E. Alessio, A. Prodi, C. Chiorboli, F. Scandola, *Inorg. Chem.* **2005**, *44*, 9752–9762.

[49] A porphyrin tape very similar to [{*t,c,c*-RuCl₂(CO)₂}₄(4′*cis*DPyMP)₂(4′TPyP)], but featuring {*fac*-ReCl(CO)₃} metal connectors, had been proposed (but, to our best knowledge, never prepared) in 2006: J. T. Hupp, *Struct. Bond.* (E. Alessio ed.) **2006**, *121*, 145–165.

[50] R. D. Sommer, A. L. Rheingold, A. J. Goshe, B. Bosnich, *J. Am. Chem. Soc.* **2001**, *123*, 3940–3952.

[51] Y.-F. Han, Y.-J. Lin, L.-H. Weng, H. Berkeab, G.-X. Jin, *Chem. Commun.* **2008**, 350–352.

[52] N. P. E. Barry, M. Austeri, J. Lacour, B. Therrien, *Organometallics* **2009**, *28*, 4894–4897.

[53] C. Garcia-Simon, M. Garcia-Borras, L. Gomez, I. Garcia-Bosch, S. Osuna, M. Swart, J. M. Luis, C. Rovira, M. Almeida, I. Imaz, D. Maspoch, M. Costas, X. Ribas, *Chem. Eur. J.* **2013**, *19*, 1445–1456.

[54] C. Garcia-Simon, M. Garcia-Borras, L. Gomez, T. Parella, S. Osuna, J. Juanhuix, I. Imaz, D. Maspoch, M. Costas, X. Ribas, *Nat. Commun.* **2014**, *5*, 5557.

[55] Y. Wang, P. L. Ang, C.-Y. Wong, J. H. K. Yip, *Chem. Eur. J.* **2018**, *24*, 18623–18628.

[56] C. Garcia-Simon, A. Monferrer, M. Garcia-Borras, I. Imaz, D. Maspoch, M. Costas, X. Ribas, *Chem. Commun.* **2019**, *55*, 798–801.

[57] A. Vidal, F. Battistin, G. Balducci, N. Demitri, E. Iengo, E. Alessio, *Inorg. Chem.* **2019**, *58*, 7357–7367.

[58] K. Araki, S. Dovidauskas, H. Winnischofer, A. D. P. Alexiou, H. E. Toma, *J. Electroanal. Chem.* **2001**, *498*, 152–160.

[59] The crystals were too few for allowing us to record an NMR spectrum immediately after re-dissolving them.

[60] E. Iengo, T. Gatti, E. Zangrando, M. T. Indelli, F. Scandola, E. Alessio, *Chem. Commun.* **2011**, *47*, 1616–1618.

[61] A. Amati, PhD Thesis in Chemistry, Cycle 31, University of Trieste (Italy), **2019**. Electronic PhD Thesis and Dissertation Repository. https://hdl.handle.net/11368/2957166.

[62] F. Scandola, C. Chiorboli, A. Prodi, E. Iengo, E. Alessio, *Coord. Chem. Rev.* **2006**, *250*, 1471–1496.

[63] M. Kasha, H. R. Rawls, M. A. El-Bayoumi, *Pure Appl. Chem.* **1965**, *11*, 371–392.

[64] N. Yoshida, T. Ishizuka, A. Osuka, D. H. Jeong, H. S. Cho, D. Kim, Y. Matsuzaki, A. Nogami, K. Tanaka, *Chem. Eur. J.* **2003**, *9*, 58–75.

[65] L. Zanetti-Polzi, A. Amadei, R. Djemili, S. Durot, L. Schoepff, V. Heitz, B. Ventura, I. Daidone, *J. Phys. Chem. C.* **2019**, *123*, 13094–13103.

[66] S. G. Telfer, T. M. McLean, M. R. Waterland, *Dalton Trans.* **2011**, *40*, 3097–3108.

[67] E. Alessio, M. Casanova, E. Zangrando, E. Iengo, *Chem. Commun.* **2012**, *48*, 5112–5114.

[68] I. Bratsos, E. Alessio, *Eur. J. Inorg. Chem.* **2018**, 2296–3013.

[69] E. Alessio, B. Milani, M. Bolle, G. Mestroni, P. Faleschini, F. Todone, S. Geremia, M. Calligaris, *Inorg. Chem.* **1995**, *34*, 4722–4734.

[70] W. Kabsch, *Acta Crystallogr. Sect. D* **2010**, *66*, 125–132.

[71] G. M. Sheldrick, *Acta Crystallogr. Sect. A* **2015**, *72*, 3–8.

[72] G. M. Sheldrick, *Acta Crystallogr.* **2008**, *64*, 112–122.

[73] P. Emsley, K. Cowtan, *Acta Crystallogr. Sect. D* **2004**, *60*, 2126–2132.

[74] C. B. Huebschle, G. M. Sheldrick, B. Dittrich, *J. Appl. Crystallogr.* **2011**, *44*, 1281–1284.

[75] A. L. Spek, *Acta Crystallogr. Sect. C* **2015**, *71*, 9–18.